Clays and Clay Minerals, Vol. 59, No. 3, 215–232, 2011.

SOLUBILITY AND THERMODYNAMIC PROPERTIES OF CARBONATE-BEARING HYDROTALCITE–PYROAURITE SOLID SOLUTIONS WITH A 3:1 Mg/(Al+Fe) MOLE RATIO

K. B. Rozov[1,2,*], U. Berner[1], D. A. Kulik[1], and L. W. Diamond[2]

[1] Waste Management Laboratory, Paul Scherrer Institute, 5210 Villigen, Switzerland
[2] Rock-Water Interaction Group, Institute of Geological Sciences, University of Bern, Baltzerstrasse 3, 3012 Bern, Switzerland

Abstract—The naturally occurring layered double hydroxides (LDH, or anionic clays) are of particular interest in environmental geochemistry because of their ability to retain hazardous cations and especially anions. However, incorporation of these minerals into predictive models of water–rock interaction in contaminant environments, including radioactive-waste repositories, is hampered by a lack of thermodynamic and stability data. To fill part of this gap the present authors have derived properties of one of the complex multicomponent solid solutions within the LDH family: the hydrotalcite–pyroaurite series, $Mg_3(Al_{1-x}Fe_x)(OH)_8(CO_3)_{0.5}\cdot 2.5H_2O$.

Members of the hydrotalcite–pyroaurite series with fixed $Mg^{II}/(Al^{III}+Fe^{III})$ = 3 and various $Fe^{III}/(Fe^{III}+Al^{III})$ ratios were synthesized by co-precipitation and dissolved in long-term experiments at 23±2ºC and pH = 11.40±0.03. The chemical compositions of co-existing solid and aqueous phases were determined by inductively coupled plasma-optical emission spectroscopy, thermogravimetric analysis, and liquid scintillation counting of ^{55}Fe tracers; X-ray diffraction and Raman were used to characterize the solids. Based on good evidence for reversible equilibrium in the experiments, the thermodynamic properties of the solid solution were examined using total-scale Lippmann solubility products, $\Sigma\Pi_T$. No significant difference was observed between values of $\Sigma\Pi_T$ from co-precipitation and from dissolution experiments throughout the whole range of Fe/Al ratios. A simple ideal solid-solution model with similar end-member $\Sigma\Pi_T$ values (a regular model with $0 < W_G < 2$ kJ mol^{-1}) was sufficient to describe the full range of intermediate mineral compositions. In turn, this yielded the first estimate of the standard Gibbs free energy of the pyroaurite end member, $G^o_{298,Pyr}$ = −3882.60±2.00 kJ/mol, consistent with $G^o_{298,Htlc}$ = −4339.85 kJ/mol of the hydrotalcite end member, and with the whole range of solubilities of the mixed phases. The molar volumes of the solid-solution at standard conditions were derived from X-ray data. Finally, Helgeson's method was used to extend the estimates of standard molar entropy and heat capacity of the end members over the pressure–temperature range 0–70ºC and 1–100 bar.

Key Words—Aqueous Solubility, Hydrotalcite, LDH, Molar Volume, Pyroaurite, Solid Solutions, Thermodynamic Modeling.

INTRODUCTION

The naturally occurring hydrotalcite–pyroaurite minerals $Mg_{1-x}(Al,Fe)_x(OH)_2(CO_3)_{x/2}\cdot nH_2O$ belong to the layered double hydroxide (LDH) family, also known as "anionic clays" (Miyata, 1983). These minerals are of particular interest in environmental geochemistry because of strong evidence that they may retain hazardous cations and especially anions (*e.g.* I^-, SeO_4^{2-}, SeO_3^{2-} TcO_4^{2-}, *etc.*) in repositories of nuclear waste (Cavani *et al.*, 1991). However, understanding their retention properties is hampered by: (1) scarce information on thermodynamic and stability properties of the compositionally complex solid solutions; and (2) lack of detailed, atomic-scale knowledge of the uptake mechanisms of cationic and anionic contaminants. The problems of retrieving and predicting these properties, which are required if LDH phases are to be included in geochemical models for nuclear-waste-disposal environments, has been addressed only recently (Cavani *et al.*, 1991; Allada *et al.*, 2005; Johnson and Glasser, 2003; Rozov *et al.*, 2010).

The LDH or hydrotalcite-like minerals can be described by the general formula $[M^{II}_{(1-x)}M^{III}_{(x)}(OH)_2]^{x+}[A^{y}_{x/y}{}^{-}\cdot nH_2O]^{x-}$. The first set of brackets represents brucite-like hydroxide layers in which divalent or trivalent metal ions (M^{II} and M^{III}) occupy the octahedral sites. The charge deficit of the octahedral sheets is compensated by interlayer anions, which are accompanied by molecules of water (second set of brackets in the formula) (Figure 1). The wide compositional ranges of these minerals are explained by: (1) ready substitution of cations with different oxidation states (Khan and O'Hare, 2002); (2) a broad possible range of cationic ratios in the formula; and (3) an ability to exchange the interlayer anions. Accordingly, LDH phases must be considered within a framework of complex multicomponent solid solutions.

* E-mail address of corresponding author:
k.rozov@fz-juelich.de
DOI: 10.1346/CCMN.2011.0590301

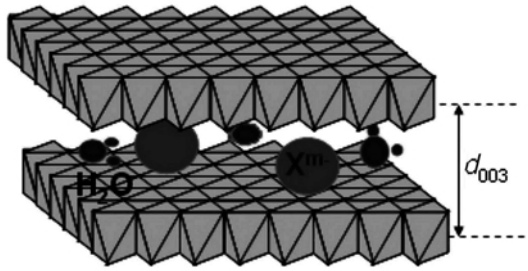

Figure 1. Structure of layered double hydroxides (LDH), showing stacking of brucite-like layers with intercalated anions and molecules of water.

The stability of LDH depends on several factors: the absolute radii of the cations, the ratios of the cations, and the types of interlayer anions. The distribution of heterovalent cations in the octahedral sheets may be completely random, ordered, or intermediate. According to Brindley and Kikkawa (1979), the distance between M^{III} ions is maximized due to cation repulsion. As an example, for LDH with a ratio of $M^{II}/M^{III} = 2$, each M^{III} ion is surrounded by six M^{II} ions and each M^{II} ion is surrounded by three M^{III} ions (Figure 2a). For LDH with $M^{II}/M^{III} = 3$, the M^{III} ions are each surrounded by six M^{II} ions, and each M^{II} ion thus has two nearest M^{III} neighbors (Drits and Bookin, 2001) (Figure 2b). In contrast, the ordering of the interlayer anions is random.

Several studies (Cavani *et al.*, 1991; Khan and O'Hare, 2002; De Roy *et al.*, 1992) revealed that LDH phases can be formed within the mole fraction range $0.20 < x < 0.33$, corresponding to M^{II}/M^{III} ratios between 2 and 4. In addition, theoretical calculations presented by Trave *et al.* (2002) showed that Mg-Al-containing LDH phases are stabilized close to $x = 0.25$, such that $M^{II}/M^{III} = 3$. Values of $x > 0.33$ (or $M^{II}/M^{III} < 2$) lead to strong charge repulsion, which renders the M^{III}–O–M^{III} bond energetically unfavorable. The stability of LDH phases with $x > 0.33$ has been confirmed only in the case of Cr^{IV}-bearing LDH (Gutmann and Müller, 1996).

A great variety of anions can be intercalated between the octahedral sheets during the formation of the LDH phases or during subsequent anion-exchange reactions. Thus, in addition to water molecules, the interlayer space may contain single anions such as Cl^- and OH^- (Chisem and Jones, 1994), triangular planar groups such as CO_3^{2-} and NO_3^- (Allada *et al.*, 2005; Chisem and Jones, 1994), tetrahedral groups such as SO_4^{2-} and CrO_4^{2-} (Brindley and Kikkawa, 1980), or octahedral groups such as $[Fe(CN)_6]^{4-}$ (Carrado *et al.*, 1988; Chibwe and Jones, 1989). A complex network of hydrogen bonds may therefore arise, joining hydroxyl groups, anions, and water molecules (Brindley and Kikkawa, 1979; Miyata, 1975). Natural LDH usually contain CO_3^{2-} and less often Cl^- and SO_4^{2-} (Cavani *et al.*, 1991; Drits *et al.*, 1987). Synthesis of CO_3^{2-}-free LDH is challenging because of the great selectivity of LDH phases for the CO_3^{2-} anion (Miyata, 1983). The relative stabilities of hydrotalcite-like phases intercalated with different anions (such as NO_3^-, CO_3^{2-}, Cl^-, and OH^-) were studied recently using calorimetric measurements (Allada *et al.*, 2005), the results of which demonstrated that carbonate-bearing hydrotalcites are less soluble than those that contain nitrates or halides.

The aim of the present work was to quantify at ambient conditions the solubility and thermodynamic properties of one of the solid-solution series within the LDH family, namely, the hydrotalcite (Htlc)–pyroaurite (Pyraur) series, $Mg_3Al(OH)_8(CO_3)_{0.5}{\cdot}nH_2O$–$Mg_3Fe(OH)_8(CO_3)_{0.5}{\cdot}nH_2O$, along which Al and Fe substitute for each other within octahedral sites. Using the results of co-precipitation (Rozov *et al.*, 2010) and dissolution experiments (present work), the following values were derived: (1) Gibbs free energies of hydrotalcite–pyroaurite end members as a function of their Fe content; and (2) total-scale Lippmann solubility products of hydrotalcite–pyroaurite solid solutions. These solubility products were used to compare the degree of oversaturation or undersaturation in aqueous solutions following the synthesis or dissolution experi-

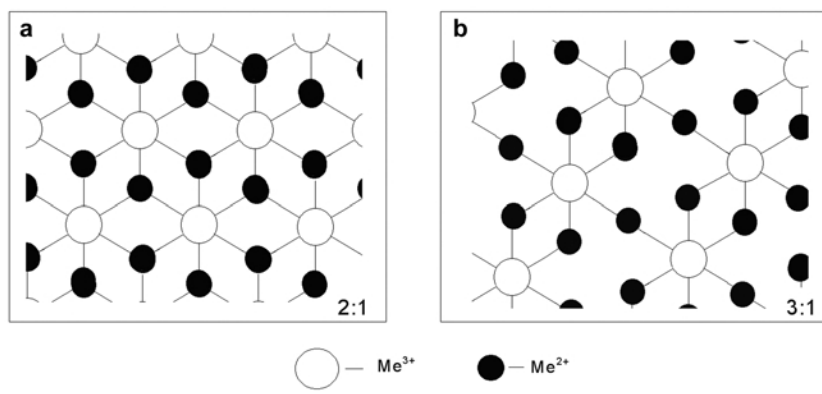

Figure 2. Possible ordering and coordination of M^{III} and M^{II} cations in brucite-like layers of LDH phases with (a) $M^{II}/M^{III} = 2{:}1$ and (b) $M^{II}/M^{III} = 3{:}1$.

https://doi.org/10.1346/CCMN.2011.0590301 Published online by Cambridge University Press

ments. Hence, compositions of the solid and aqueous phases at equilibrium could be predicted and the appropriateness of the selected solid-solution model could be tested.

In a previous study (Rozov *et al.*, 2010), large uncertainties in the derived Gibbs free energies (and excess free energies of mixing) were shown to possibly arise from analytical uncertainties in the composition of the solid phase. Evaluating the degree of non-ideality of the solid solution and selecting an appropriate descriptive model, therefore, become difficult. Additional analytical techniques were used in the present study to better characterize the aqueous solution of the hydrotalcite-pyroaurite system. In particular, ^{55}Fe radiotracers were introduced into the setup and then liquid scintillation counting was performed to determine more accurately the total dissolved Fe after the co-precipitation and dissolution experiments. The advantage of this method is its high sensitivity (*e.g.* compared to inductively coupled plasma optical emission spectroscopy – ICP-OES), especially in solutions with large Na contents (0.1–0.2 mol/L). Unfortunately, Al and Mg radiotracers were unavailable at the time of this study. The solid products were also characterized by powder X-ray diffraction (XRD), Raman spectroscopy, and thermogravimetric analysis.

Solubility properties, including thermodynamic and total solubility products, of the hydrotalcite–pyroaurite series in terms of standard molar Gibbs free energies of end members are presented here. All of these properties are consistent with the GEMS version of the *NAGRA-PSI 01/01 Chemical Thermodynamic Database* (Hummel, 2002).

METHODS

LDH synthesis

Members of the hydrotalcite–pyroaurite series with $Mg^{II}/(Al^{III}+Fe^{III})$ mole ratio $\approx$ 3:1 were synthesized by a co-precipitation method at ambient temperature and pH = 11.40±0.03. A metal nitrate solution with the desired $Mg^{2+}/(Al^{3+}+Fe^{3+})$ ratio was added slowly to a stirred reactor containing Na_2CO_3 solution under a nitrogen atmosphere at controlled pH. Crystals of 10–30 μm diameter were obtained. The procedure was described in detail by Rozov *et al.* (2010).

A similar method was used to dope the same solid-solution series with ^{55}Fe tracers. The syntheses were performed in 40 mL centrifuge vials containing 20.075 mL of 0.025 M Na_2CO_3 solution. Small amounts of ^{55}Fe-labeled solutions (0.665 mL, which corresponds to 3.36×10^6 Bq) were added to the metal-nitrate solution before synthesis. During the synthesis, the metal-nitrate solution was added at a rate of 0.02 mL/min (6.014 mL). The pH value was controlled by simultaneous addition of 2 M NaOH (maximum rate 0.05 mL/min). After the addition step, the suspension was aged for 24 h with continuous stirring at controlled pH. The precipitate was washed and separated as described by Rozov *et al.* (2010). After the experiments, the concentration of dissolved Fe was measured by liquid scintillation counting (LSC). Dissolved Mg, Al, Na, NO_3^-, and CO_3^{2-} were not analyzed in these traced runs. Instead, their concentrations and the stoichiometric compositions of the precipitates were assumed to be the same as those in the parallel experiments without the ^{55}Fe tracer.

Dissolution experiments

Prior to the dissolution experiments, the solid phases were dried at 60ºC for 24 h in order to remove physically adsorbed water. The solutions used for the dissolution experiments were pre-conditioned by adding 2 M NaOH to degassed MilliQ water using a Metrohm® Titroprocessor 670 unit until the desired pH value was reached. The solutions and solids were then placed in 50 mL glass flasks (liquid:solid ratio = 409.1±22.8). The flasks were kept on stirring devices for the entire equilibration time ($\geqslant$140 days). After equilibration, the suspensions were centrifuged in 40 mL Beckmann Coulter® centrifuge tubes at $95{,}000\times g$ for 1.5 h. Parallel dissolution experiments using ^{55}Fe-spiked precipitates were carried out directly in centrifuge tubes at pH = 11.40±0.03.

Chemical analyses of solid and liquid phases

The contents of Mg, Al, Fe, and Na in the solid and liquid phases were determined by ICP-OES using a Perkin-Elmer® Vista Pro instrument. The uncertainty of the concentrations in the solids is <±5% for Mg, Al, and Fe, and the uncertainty for total Mg, Al, and Fe in the experimental liquid phases is ~±50%. Nitrate anions in the liquid phase were analyzed spectrophotometrically after separation by ion chromatography (Dionex® DX-600 instrument with Ionpac® AS16/AG16 chromatograph columns). The carbonate content in the liquid phase was determined using a Shimadzu® TOC-V analyzer. Details are given in Rozov *et al.* (2010).

Liquid scintillation counting (LSC)

Samples were prepared by mixing 5 mL of the supernatant solution from the dissolution experiments with 15 mL of scintillation cocktail (high flash-point Perkin-Elmer® Ultima Gold XR) in the beta-vials. Measurements were carried out using a PACKARD® TRI-CARB 2250 liquid scintillation analyzer at ambient conditions (23±2ºC). Calibration solutions were prepared using an ^{55}Fe isotope standard (Ecker & Ziegler Isotope Products®) in an NaOH solution with pH = 11.40±0.02.

Powder X-ray diffraction

Solids produced in the synthesis and dissolution experiments were analyzed directly by powder XRD

https://doi.org/10.1346/CCMN.2011.0590301 Published online by Cambridge University Press

using a Panalytical® X'Pert Pro diffractometer equipped with a CuKα radiation source. The XRD patterns were acquired at ambient temperature within a 2θ range from 5 to 70º, using a step size of 0.0168º and a counting time of ~0.31 s per step. No internal standards were used to detect possible peak offsets. The limit of detection is ~5–6 wt.% of the sample. Details of the evaluation of cell parameters were given by Rozov *et al.* (2010).

Raman spectroscopy

Raman spectroscopic measurements were carried out to identify the interlayer anions in the LDH minerals. Raman scattering spectra were acquired by irradiating the samples with a 532.12 nm (green) frequency-doubled Nd-YAG laser through an Olympus BX41 petrographic microscope. The measurements were made using a Jobin Yvon Horiba® Labram HR 800 instrument equipped with a 1800 groove/mm grating. This setup yielded a spectral resolution of ~1 cm^{-1}. The sample preparation and band-component analysis were described by Rozov *et al.* (2010).

Thermogravimetric analyses (TGA)

The TGA was carried out in order to determine the amount of interlayer water and of hydroxide and carbonate anions in the solids. Measurements were performed using a Mettler Toledo® TGA device. Before the measurements, the samples were dried at 60ºC for 15 min. With this procedure, the solid was brought to the same conditions as it was after co-precipitation and drying at 60ºC for 24 h. The weight loss of the solids in air was then analyzed from 60ºC to 1000ºC with a heating rate of 5ºC/min. Uncertainties in the determination of CO_3 in the solids were ~±2%.

THERMODYNAMIC DESCRIPTION OF HYDROTALCITE–PYROAURITE SOLID SOLUTION–AQUEOUS SOLUTION SYSTEMS

Estimation of molar Gibbs free energy of hydrotalcite–pyroaurite solid solutions

Molar Gibbs free energies (G_{298}) of the hydrotalcite–pyroaurite series were estimated from equilibrium solution compositions according to the following scheme: (1) the aqueous solutions obtained from the synthesis (Rozov *et al.*, 2010) and dissolution experiments (Table 1) were modeled using the Gibbs free energy minimization software *GEM-Selektor* (http://gems.web.psi.ch), which includes the thermodynamic data in Hummel (2002); (2) from the calculated chemical potentials of Mg^{2+}, Al^{3+}, Fe^{3+}, OH^-, and CO_3^{2-} in the aqueous phase and from the stoichiometric coefficients of the synthesized solids (Rozov *et al.*, 2010) and solid products of dissolution experiments (Table 2), the molar Gibbs free energies of formation of water-free compositions were obtained from the following equilibrium relation:

$$G_{298}(\text{Htlc-Pyraur}) = a\mu(Mg^{2+}) + b\mu(Al^{3+}) + c\mu(Fe^{3+}) + d\mu(OH^-) + e\mu(CO_3^{2-}) \quad (1)$$

where μ is the calculated chemical potential of the bracketed aqueous species, and indexes *a* to *e* are the stoichiometric reaction coefficients, based on the analyses of the solid phases. The attainment of equilibrium during the experiments is demonstrated in the results section below.

Uncertainties in the calculated G_{298} values have been evaluated by propagating the analytical errors associated with the compositions of the solid and liquid phases. A

Table 1. Compositions of solutions after dissolution experiments at 23±2ºC and pH = 11.40±0.03.

$x^{a}_{Fe,\ solid}$	Equilibration time (days)	Mg	Al	Fe		Na	CO_3^{2-}	Mole ratio Mg/(Al+Fe)	$x_{Fe,aq}$
				ICP-OES[b]	LSC[c]			in aqueous solution	
		μmol/kg				mmol/kg			
0	91	2.96	1.39	0.00	–	2.32	<0.01	2.13	0.00
0	115	17.60	6.01	0.00	–	2.39	<0.01	2.92	0.00
0	141	34.80	11.60	0.00	–	2.51	<0.01	2.99	0.00
0.2	133	20.50	5.26	1.45	0.30	2.17	<0.01	3.06	0.22
0.2	189	10.60	1.65	0.45	0.30	2.24	<0.01	5.01	0.21
0.5	189	18.80	2.67	2.67	1.36	2.20	<0.01	3.74	0.5
0.6	160	79.80	13.10	15.50	0.07	2.69	<0.011	2.79	0.54
0.7	160	30.40	3.68	7.10	0.96	2.66	<0.01	2.82	0.66
0.8	133	15.10	1.50	3.27	1.78	2.19	<0.01	3.17	0.69
0.8	189	7.68	0.30	0.87	1.78	2.24	<0.01	6.55	0.74
0.9	160	42.20	1.73	11.60	–	2.63	<0.01	3.17	0.87
1	91	10.90	0.00	2.78	1.50	2.33	<0.01	3.26	1.00
1	115	19.50	0.00	5.27	1.50	2.46	<0.01	3.71	1.00
1	141	9.09	0.00	1.82	1.50	2.34	<0.01	5.01	1.00

[a] Approximate mole fraction of Fe in solid phase; [b] analyzed by ICP-OES;
[c] analyzed in parallel experiments using liquid scintillation counting of ^{55}Fe tracers.

https://doi.org/10.1346/CCMN.2011.0590301 Published online by Cambridge University Press

Table 2. Stoichiometric formulae, estimated standard Gibbs free energies and total-scale Lippmann solubility products of solids after dissolution experiments.

Mole ratio Fe/(Fe+Al) in solid, $x_{Fe,\ solid}$	Stoichiometric formulae (without interlayer water)	Time (days)	Molar ratio $Mg^{2+}/(Al^{3+}+Fe^{3+})$ in solid	G_{298} [kJ/mol] (without interlayer H_2O) ICP-OES[a]	LSC[b]	$\log\Sigma\Pi_T$ ICP-OES[a]	LSC[b]
0.000	$Mg_{3.000}Al_{0.983}(CO_3)_{0.593}(OH)_{7.764}$	91	3.051±0.304	−3768.35±113.00	No data	−35.3±1.3	No data
0.000	$Mg_{3.000}Al_{0.981}(CO_3)_{0.592}(OH)_{7.759}$	115	3.058±0.305	−3748.99±115.00	No data	−32.3±1.3	No data
0.000	$Mg_{3.000}Al_{0.948}(CO_3)_{0.518}(OH)_{7.808}$	141	3.164±0.317	−3689.42±110.49	No data	−31.1±1.3	No data
0.198±0.025	$Mg_{3.000}Al_{0.769}Fe_{0.190}(CO_3)_{0.355}(OH)_{8.168}$	133	3.128±0.251	−3582.13±103.93	−3583.00	−32.1±1.2	−32.1
0.189±0.025	$Mg_{3.000}Al_{0.791}Fe_{0.184}(CO_3)_{0.351}(OH)_{8.223}$	189	3.077±0.256	−3610.43±106.23	−3610.90	−33.5±1.2	−33.5
0.509±0.063	$Mg_{3.000}Al_{0.489}Fe_{0.507}(CO_3)_{0.427}(OH)_{8.134}$	189	3.012±0.215	−3496.82±96.77	−3500.14	−32.6±1.2	−32.5
0.591±0.073	$Mg_{3.000}Al_{0.388}Fe_{0.560}(CO_3)_{0.654}(OH)_{7.537}$	160	3.165±0.227	−3447.38±90.32	−3454.99	−29.6±1.2	−29.9
0.692±0.087	$Mg_{3.000}Al_{0.294}Fe_{0.659}(CO_3)_{0.659}(OH)_{7.541}$	160	3.148±0.238	−3419.58±87.46	−3422.63	−31.3±1.2	−31.3
0.791±0.103	$Mg_{3.000}Al_{0.202}Fe_{0.766}(CO_3)_{0.143}(OH)_{8.619}$	133	3.099±0.256	−3286.83±81.29	−3287.80	−32.7±1.2	−31.6
0.796±0.101	$Mg_{3.000}Al_{0.200}Fe_{0.779}(CO_3)_{0.173}(OH)_{8.590}$	189	3.064±0.247	−3307.60±82.53	−3306.78	−34.2±1.2	−33.92
0.898±0.122	$Mg_{3.000}Al_{0.097}Fe_{0.857}(CO_3)_{0.396}(OH)_{8.071}$	160	3.145±0.287	−3271.03±77.75	No data	−30.8±1.2	No data
1.000	$Mg_{3.000}Fe_{1.007}(CO_3)_{0.843}(OH)_{7.335}$	91	2.979±0.281	−3374.17±73.00	−3376.48	−33.3±1.3	No data
1.000	$Mg_{3.000}Fe_{0.949}(CO_3)_{0.280}(OH)_{8.285}$	115	3.161±0.316	−3206.26±72.85	−3209.77	−32.2±1.3	No data
1.000	$Mg_{3.000}Fe_{0.960}(CO_3)_{0.298}(OH)_{8.285}$	141	3.125±0.313	−3218.47±73.88	−3227.43	−33.7±1.3	No data

[a] Analyzed by ICP-OES; [b] analyzed in analogous parallel experiments using liquid scintillation counting of ^{55}Fe tracers.

set of limiting combinations of stoichiometric coefficients of Mg, Al, Fe, CO_3, and OH in the solids was established, such that the analytical errors do not exceed ±5% for Mg, Al, and Fe and ±2% for the CO_3 group. This leads to the 16 combinations in Figure 3. For each combination, the OH^- content was calculated by difference to maintain overall charge balance. Values of G_{298} were then calculated for each of the 16 resulting stoichiometries of equation 1, such that the concentrations of aqueous Mg, Al, and Fe could be reproduced within their ±50% errors. For a given reaction stoichiometry, G_{298} had to be varied by only ±2–3 kJ/mol in order to reproduce all the solute concentrations except for Mg. The calculated total Mg concentrations were always slightly less than the −50% limit of the analytical uncertainty. This may be due to the formation of small amounts of brucite during the dissolution experiments which were not detectable by XRD analysis (L.O.D. <5–6 wt.%). The range of feasible G_{298} values for all 16 combinations is −3419.50 to −3214.35 kJ/mol (*i.e.* the error is ±103 kJ/mol). This underscores how small changes in the composition of the solid result in huge variations in the molar Gibbs free energy of the solid solution.

Estimation of the total-scale Lippmann solubility product

To assess whether hydrotalcite–pyroaurite solid solutions can be considered ideal or non-ideal and to reconcile them with the analytical data from co-precipitation and dissolution experiments, Lippmann functions and diagrams (Lippmann, 1980) have been

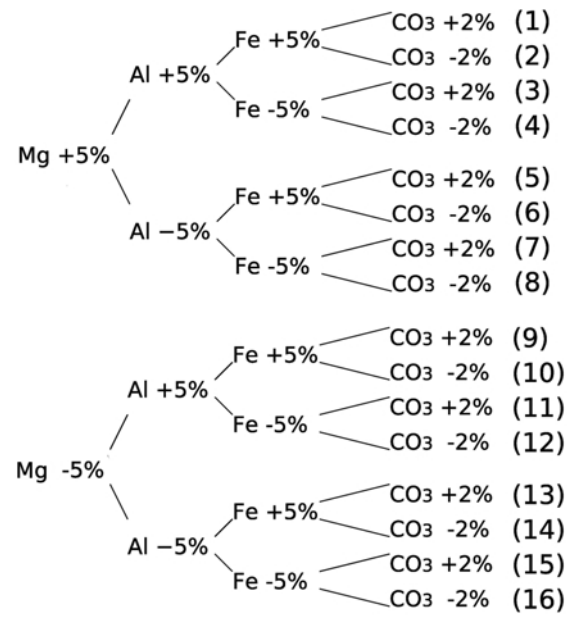

Figure 3. Combinations of analytical uncertainty limits for Mg, Al, Fe, and CO_3 in hydrotalcite–pyroaurite solid solutions.

https://doi.org/10.1346/CCMN.2011.0590301 Published online by Cambridge University Press

used. 'Classic' Lippmann diagrams are based on the 'total solubility product,' $\Sigma\Pi$, defined in terms of aqueous activities of substituting ions and the common counter-ions. In the present case, $\Sigma\Pi$ would include the sum of activities of Fe^{3+} and Al^{3+} ions times the activity of carbonate and hydroxyl ions with their respective power coefficients. However, thermodynamic modeling of relevant alkaline systems at pH = 11.40 indicated that the speciation of Al and Fe is dominated (~99%) by $Al(OH)_4^-$ and $Fe(OH)_{4i}^-$ species, and that the activities of the simple ions (Al^{3+} and Fe^{3+}) are immeasurably low (10^{-35}–10^{-28}). Therefore, from a mass-balance point of view, it makes sense to express the Lippmann solubility products of the hydrotalcite–pyroaurite series in terms of the concentrations of Al_{aq} and Fe_{aq} actually measured (equation 2). In contrast, Mg^{2+} can be taken to represent Mg_{aq}, because thermodynamic modeling showed that the Mg^{2+} species is dominant (~60% of total dissolved Mg corresponds to Mg^{2+}) even at high pH. Accordingly, the Lippmann diagrams in this study were constructed in the total concentration scale by using concentrations of total dissolved Mg, Al, Fe, and C (indexed with aq), with the term (pH − 14) representing the logarithmic concentration of hydroxyl, OH^-:

$$\log_{10}\Sigma\Pi_T = \log_{10}([Mg_{aq}]^a([Al_{aq}] + [Fe_{aq}])^{(b+c)}[C_{aq}]^e) + (d - 4(b + c))\cdot(pH - 14) \quad (2)$$

Solidus and solutus data are presented on the total-scale Lippmann diagram with the common ordinate $\Sigma\Pi_T$ and two abscissas. The solutus data are plotted against the aqueous mole fraction of Fe with respect to the total ions available for substitution in the octahedral sites:

$$x_{Fe,aq} = \frac{[Fe_{aq}]}{([Fe_{aq}] + [Al_{aq}])} \quad (3)$$

The solidus data are plotted against the analogous mole fraction of Fe in the solid solution:

$$x_{Fe,solid} = \frac{n_{Fe}}{(n_{Fe} + n_{Al})} \quad (4)$$

where n_{Fe} and n_{Al} are the moles of Fe and Al in the solid.

RESULTS AND DISCUSSION

Characterization of solid products from co-precipitation and dissolution experiments by powder XRD

All precipitates display powder XRD patterns typical of pure hydrotalcite-like phases (Figure 4). All observed peaks can be assigned on the basis of a hexagonal cell with a_o being the shortest cation–cation distance and c_o corresponds to the three-layer rhombohedral polytype 3*R*. Each of these layers (c_o/3) consists of a brucite-like layer and one interlayer.

Unit-cell distances were estimated from peak-profile analysis using a Bragg-type evaluation (Rozov *et al.*, 2010). None of the patterns showed any secondary phase, *i.e.* the amounts of any conceivable impurities in the solids (such as gibbsite, brucite, magnesite, or ferric hydroxides) were less than the detection limit of the XRD technique (~5–6 wt.%) (Bish and Howard, 1988).

The unit-cell parameters ($a_o = b_o$, c_o) of the end members are represented as a function of time in the dissolution experiment (Figure 5), which revealed that unit-cell distances $a_o = b_o$ did not change significantly during the 140 days of the dissolution experiment. In the same time period, the interlayer distance, c_o, decreased by <0.03 Å per interlayer, indicating that the number of interlayer water molecules remained nearly constant (note that one layer of interlayer water adds ~2–3 Å to the length of c_0). Hence, the *M*(II)/*M*(III) ratio in the brucite-like layer appeared to remain approximately

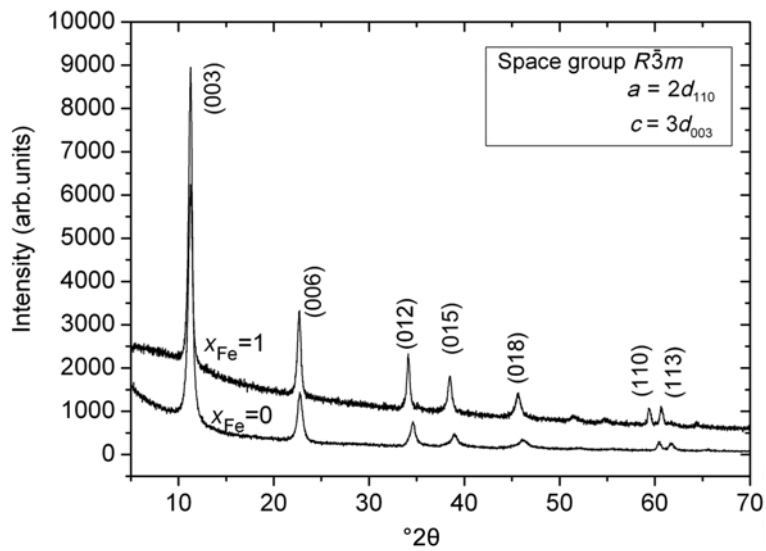

Figure 4. XRD patterns of hydrotalcite ($x_{Fe,\ solid}$ = 0) and pyroaurite ($x_{Fe,\ solid}$ = 1) samples.

https://doi.org/10.1346/CCMN.2011.0590301 Published online by Cambridge University Press

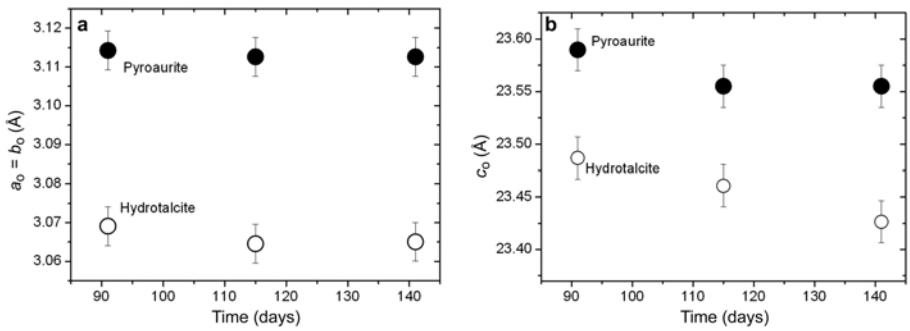

Figure 5. Unit-cell parameters of hydrotalcite and pyroaurite as a function of time during the dissolution experiments: (a) $a_o = b_o$, (b) c_o.

constant. The very small changes in the c_o parameter, which lie only slightly outside the analytical uncertainties, indicated, at most, insignificant rearrangements/substitutions of interlayer anions (*i.e.* substitutions of carbonate by hydroxide).

The observed variation in $a_o = b_o$ as a function of $x_{Fe,\,solid}$ (Figure 6) is in good agreement with Vegard's law (Danton, 1991), confirming the presence of a continuous solid solution throughout the hydrotalcite–pyroaurite series and the absence of a miscibility gap. Linear regression analysis found that:

$$a_o = (3.063\pm0.001)+(0.048\pm0.001)\cdot x_{Fe,solid}\ (\text{Å}),\ R^2 = 0.976$$

Using this linear regression, the $a_o = b_o$ cell parameters for hydrotalcite and pyroaurite end members were estimated to be:

$a_o = b_o$ (hydrotalcite) = 3.063±0.001 Å;
$a_o = b_o$ (pyroaurite) = 3.111±0.002 Å

These unit-cell distances agreed well with the data presented in other studies: for pyroaurite $a_o = b_o$ = 3.109 Å, (Allmann, 1968); for hydrotalcite $a_o = b_o$ = 3.061 Å (Prikhod'ko *et al.*, 2001), and $a_o = b_o$ = 3.054 Å (Kovanda *et al.*, 2005).

The length c_o depends on the layer-charge density, the nature of the interlayer anion (CO_3^{2-}), and the number of water molecules in the interlayer space. As demonstrated in Figure 7 and Table 3, the cell parameter c_o does not change significantly as a function of $x_{Fe,\,solid}$. The slight increase of each $c_o/3$ layer from 7.782 to 7.863 Å can be attributed to replacement of the smaller Al^{III} (r^{III}_{Al} = 0.535 Å) by the larger Fe^{III} (r^{III}_{Fe} = 0.645 Å). The absolute values 7.782 and 7.863 Å are consistent with the assumed structure of the interlayer, comprising flat CO_3 groups and not more than two layers of water. This interpretation is also consistent with the results of the chemical analyses which showed a nearly constant

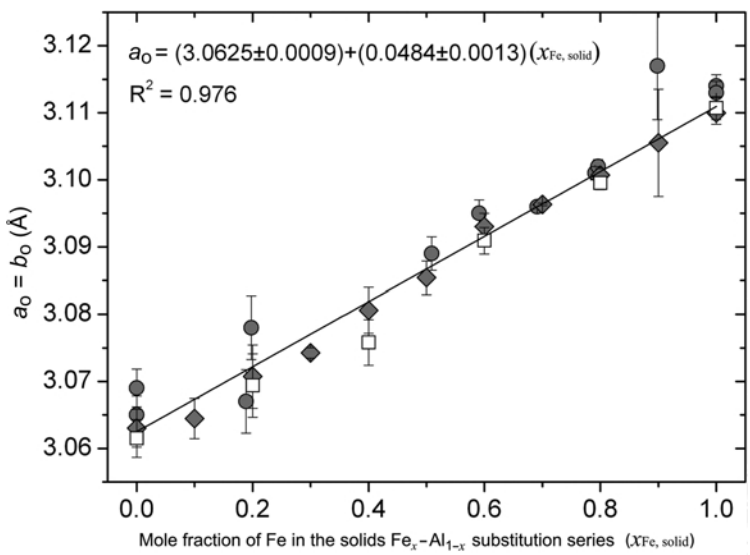

Figure 6. Unit-cell parameters $a_o = b_o$ of the hydrotalcite–pyroaurite solid solution as a function of the mole fraction of Fe ($x_{Fe,\,solid} = n_{Fe}/(n_{Fe} + n_{Al})$). Filled diamonds represent parameters of the solids following co-precipitation experiments; filled circles represent parameters of the solid products following the dissolution experiments. Open squares represent parameters determined from XRD peak-profile analysis.

https://doi.org/10.1346/CCMN.2011.0590301 Published online by Cambridge University Press

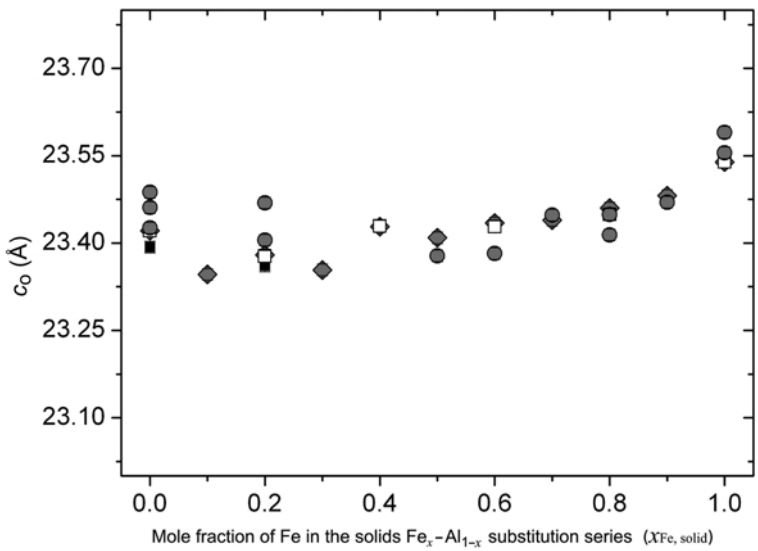

Figure 7. Dependence of the unit-cell parameter, c_o, on the mole fraction of Fe. Filled diamonds represent parameters of solid phases after co-precipitation experiments; filled circles represent parameters of solid products after dissolution experiments. Open squares represent parameters determined from XRD peak-profile analysis.

$Mg^{II}/(Al^{III}+Fe^{III})$ ratio and no significant change in the interlayer composition (Table 2).

The average particle size of 'pure' hydrotalcite and pyroaurite samples has been estimated by the Debye-Scherrer equation:

$$D_c = \frac{K\lambda}{\beta \cos\theta} \quad (5)$$

where D_c is the average particle size; β is the full-width at half maximum (FWHM) of the observed diffraction peak, expressed in radians; K is a dimensionless parameter, the so-called shape factor, which usually has a value of ~0.8–0.9; λ is the wavelength of the X-ray source used to obtain the XRD pattern; and θ is the position of the diffraction peak.

The average crystallite size of hydrotalcite and pyroaurite decreased (Figure 8) during the 140 days of the dissolution experiment (from 22 to 17 nm and from 14 to 12 nm, respectively). The size evidently did not change further after this period, indicating that the systems were close to equilibrium after ~140 days. Moreover, data in row 3 of Table 1 demonstrate that the Mg/Al ratio in the aqueous phase reached a constant value of 2.99 after the same period, additional evidence that the system was very close to the equilibrium state after 140 days.

Table 3. Cell parameters of solids after dissolution experiments determined from Bragg evaluation and refined in the space group $R\bar{3}m$.

Approx. mole ratio Fe/(Fe+Al) in solid, $x_{Fe, solid}$	Duration of experiment (days)	$a_o = b_o$ (Å)	c_o (Å)
0.00	91	3.069±0.003	23.49±0.01
0.00	115	3.065±0.003	23.46±0.01
0.00	141	3.065±0.003	23.43±0.01
0.20	133	3.078±0.005	23.47±0.01
0.20	189	3.067±0.005	23.41±0.01
0.50	189	3.089±0.003	23.38±0.01
0.60	160	3.095±0.002	23.38±0.01
0.70	160	3.096±0.002	23.45±0.01
0.80	133	3.101±0.001	23.41±0.01
0.90	160	3.117±0.008	23.47±0.01
1.00	91	3.114±0.002	23.59±0.01
1.00	115	3.113±0.002	23.56±0.01
1.00	141	3.113±0.002	23.56±0.01

https://doi.org/10.1346/CCMN.2011.0590301 Published online by Cambridge University Press

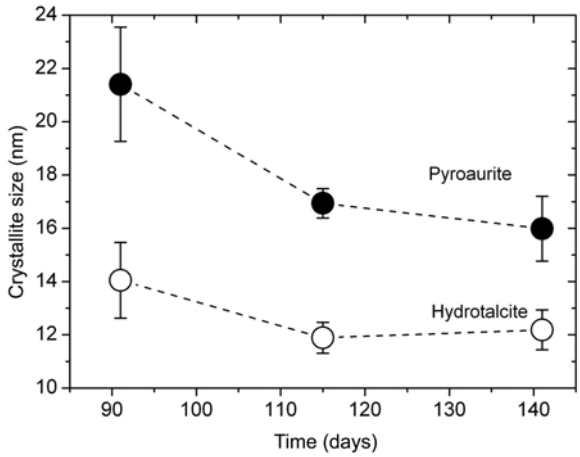

Figure 8. Crystallite size of hydrotalcite and pyroaurite samples as a function of the duration of the dissolution experiments.

Characterization of products of dissolution experiments by Raman spectroscopy

Raman spectra for the hydrotalcite–pyroaurite series with $x_{Fe,\ solid} \leqslant 0.5$ were given by Rozov *et al*. (2010). Measurements with greater Fe contents were precluded by fluorescence. The acquired spectra revealed bands around 540 cm^{-1}, 1060 cm^{-1}, 1380 cm^{-1}, and 3500 cm^{-1}, all of which are typical of a hydrotalcite-like phase with $x_{Fe,\ solid} \leqslant 0.5$ (Frost and Reddy, 2006). The band around 540 cm^{-1} originates from a carbonate–water vibration in the interlayer, where two hydrogen atoms of the H_2O molecule are bridged to two oxygen atoms of the carbonate. Thus, CO_3^{2-} was indicated in the interlayer. The band around 1060 cm^{-1} represents interlayer carbonate associated with $[M(II), M(III)](OH)_6$ octahedral units of the brucite-like layer. The band around 1380 cm^{-1} also belongs to carbonate anions, either free or bound to interlayer water molecules or to hydroxide groups of the brucite-like layer. The broad peak around 3500 cm^{-1} represents OH-stretching vibrations from OH groups and interlayer water molecules.

No bands were found that might indicate the presence of other interlayer anions such as nitrate. The interlayer space thus appeared to be occupied by CO_3 and H_2O only.

Results of dissolution experiments (solid- and liquid-phase compositions)

The compositions of the liquid and solid phases following the dissolution experiments are provided in Tables 1 and 2. The determination of stoichiometric coefficients of the solid phases were outlined by Rozov *et al.* (2010). The average $Mg^{II}/(Al^{III}+Fe^{III})$ ratio in the solids was 3.107±0.060 (Table 2). Analyses of hydroxide and carbonate were remarkably constant throughout the whole range from hydrotalcite to pyroaurite. Each formula unit contained 0.45±0.20 CO_3^{2-} and 8.01±0.39 OH^-. In addition, rinsed solids contained only traces of Na (<0.1 wt.%), which means that the stoichiometric coefficient of sodium in the hydrotalcite–pyroaurite formula was $<Na_{0.001}$ (Table 2).

Dissolution experiments were carried out at a much lower ionic strength (0.002 mol/kg) than the co-precipitation experiments (0.1–0.2 mol/kg). Measured concentrations of Mg, Al, and Fe ranged between 0.30–79.80 µmol/kg (Table 1), meaning that analytical errors for these metals were >±5%. The Mg, Al, and Fe molal concentrations varied over the ranges 2.96–79.80 µmol/kg, 0.30–13.10 µmol/kg, and 0.45–15.50 µmol/kg, respectively, but showed no trend as a function of $x_{Fe,\ solid}$, as might be expected from chemical considerations. Hence, the analytical errors for Mg, Al, and Fe were apparently substantially greater than 5%, probably ±50% or more. At the same time, dissolved Fe concentrations measured by LSC varied within a narrower range, from 0.07 to 1.78 µmol/kg. Moreover, as seen in Tables 1 and 4, Fe concentrations measured by LSC were, on average, ~50% smaller than those measured by ICP-OES in experiments without ^{55}Fe tracers (with the exception of row 10 in Table 1). Measurements of internal Fe standards for LSC revealed a precision of ~±5–10%, which rendered this technique appropriate for small concentrations of Fe (0.1–1 µmol/kg).

Estimation of end-member Gibbs free energies, parameters of mixing, and total-scale Lippmann solubility products of hydrotalcite–pyroaurite solid solutions

Given the evidence that the solids were in thermodynamic equilibrium with their coexisting aqueous solutions, the standard molar Gibbs free energies (G^o_{298}) and solubility products of hydrotalcite and

Table 4. Total dissolved Fe molalities in aqueous solutions after synthesis at 23±2°C and pH = 11.40±0.03 according to results obtained by ICP-OES and LSC techniques ($x_{Fe,\ solid}$ is the approximate mole fraction of Fe in the solid phase).

$x_{Fe,\ solid}$	— *m*Fe (µmol/kg) —	
	ICP-OES	LSC
0.0	bdl	No data
0.0	bdl	No data
0.1	0.28	0.28
0.2	1.67	0.12
0.2	bdl	0.12
0.3	0.09	No data
0.4	2.73	1.03
0.5	1.68	0.27
0.6	3.77	0.11
0.7	2.46	1.65
0.8	4.92	1.30
0.9	2.67	No data
1.0	4.68	4.03

bdl: below detection limit

https://doi.org/10.1346/CCMN.2011.0590301 Published online by Cambridge University Press

pyroaurite end members, as well as the regular interaction parameter for the excess free energy of mixing within the solid solution, were estimated.

Using the methods described in previous sections and with reference to equation 1, the following provisional values for water-free end member compositions were obtained:

$$G^{o}_{298}\text{ (hydrotalcite)} = -3746.4\pm29.5\text{ kJ/mol} \quad (6)$$
$$G^{o}_{298}\text{(pyroaurite)} = -3304.01\pm50.2\text{ kJ/mol} \quad (7)$$

As demonstrated previously, the great uncertainties in these estimates arose mainly from analytical uncertainties in the solid compositions. If the measured solid composition were taken 'as is' and uncertainties of molar Gibbs free energies derived from uncertainties of solute concentrations only (based on realistic assumption of ±50% errors for Mg, Al, and Fe), uncertainty ranges in the order of ±2−3 kJ/mol would be achieved. However, the Gibbs free energies of ideal mixing, as well as Gibbs excess energies of non-ideal mixing, are usually <5 kJ/mol at ambient temperatures (23±2ºC), meaning that even if these smaller uncertainties were valid, distinguishing clearly between ideal and non-deal solid-solution behavior would not be possible. Because a mechanical mixture was ruled out by the correspondence with Vegard's law, the available data are suggested to be

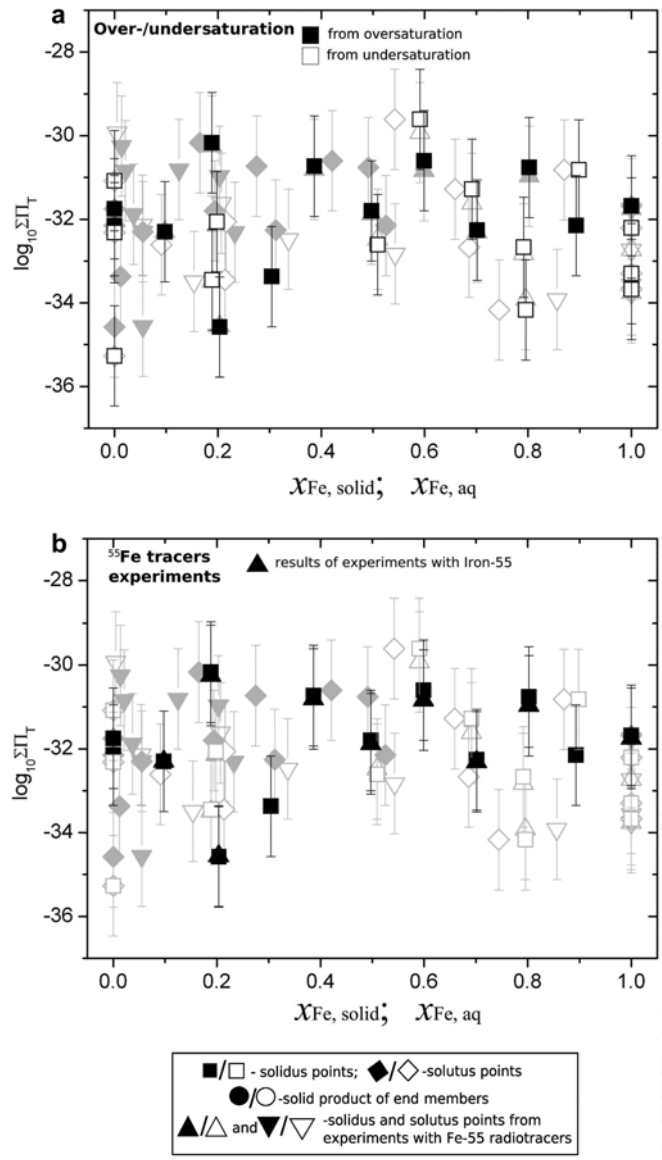

Figure 9. Measured values of total-scale Lippmann solubility products, $\Sigma\Pi_T$, of the hydrotalcite−pyroaurite solid solutions: (a) results obtained from oversaturation (co-precipitation) and undersaturation (dissolution experiments); (b) results from experiments using ^{55}Fe radiotracers. Points not relevant to the item discussed in the figure are presented in light gray.

https://doi.org/10.1346/CCMN.2011.0590301 Published online by Cambridge University Press

compatible with, but not diagnostic of, an ideal solid solution.

When the experimental data were plotted within Lippmann diagrams (Figure 9), clearly no direct relation between $\log\Sigma\Pi_T$ and the type of the experiment (whether co-precipitation or dissolution) was observed. Much of the scatter was attributed to the analytical uncertainties in Mg_{aq} and pH, as these variables have exponents of 3 and 4 in the definition of $\Sigma\Pi_T$ (equation 2). In fact, the results of both the co-precipitation and the dissolution experiments fell into the same range in Figure 9, suggesting that no significant oversaturation occurred in the co-precipitation experiments, and likewise no significant undersaturation in the dissolution experiments. Effectively, this means that co-precipitation after reaction times of ~1 week produces hydrotalcite-like solids that are close to equilibrium. In turn, this obviates the need for expensive long-term dissolution experiments to determine the thermodynamic properties of hydrotalcite–pyroaurite solid solutions.

The total-scale Lippmann solubility products of hydrotalcite–pyroaurite phases based on the co-precipitation and dissolution experiments using ^{55}Fe tracers (Figure 9b) revealed solubility products comparable to those from the experiments using ordinary analyses for dissolved Fe (this is also demonstrated in Tables 1 and 4, which list the analytical results for dissolved Fe using LSC). The radiotracer technique generally confirmed the Fe concentrations determined by 'classical' ICP-OES, although the results using the tracer have smaller uncertainties. Concentrations of all non-Fe solutes were taken from the parallel tracer-free experiments, so as to avoid the demanding operational procedures required for radioactive samples. Hence, only limited improvement was achieved by applying the radiotracer technique. Presumably additional improvement would be gained if Al and Fe tracers were used simultaneously.

The range of solubility products of the end members has been estimated to permit an attempt to reproduce the analytically measured composition of the aqueous solution at experimental conditions (T = 23±2ºC, pH = 11.40±0.03). To perform this estimate, solutions produced during the dissolution experiments were selected because these closely represent thermodynamic equilibrium. In the pyroaurite end member, the carbonate content was smaller (0.298 CO_3 groups per formula unit) than in the hydrotalcite end member (0.518 CO_3 groups) and lies close to the expected value of 0.5. As the two end members had different carbonate contents, the solid solution could not be treated as a simple binary. Therefore, several defined compositions with constant concentrations of interlayer carbonate were used for the subsequent calculations: (1) a hydrotalcite with the nominally ideal formula, *i.e.* $Mg_3(Al, Fe)(CO_3)_{0.5}(OH)_8$ (Solution I; row 1 in Table 5); (2) an Fe_x–Al_{1-x} solid solution with the concentration of carbonate equal to that measured in the hydrotalcite end member (Solution II; row 2 in Table5); (3) the analogous case with carbonate equal to that found in the pyroaurite end member (Solution III; row 3 in Table 5); and (4) a solid solution with the average (0.408) of the observed carbonate concentrations (Solution IV; row 4 in Table 5). For each of these four solid-solutions the average stoichiometric coefficients for Mg, Al, and Fe were used and the OH concentrations were calculated by charge-balance.

In the next step, the compositions of aqueous solutions produced during the 140-day dissolution experiments (rows 3 and 14 in Table 1) were modeled using the *GEM-Selektor* code to obtain activities, chemical potentials, and the speciation of all relevant components. The standard molar Gibbs free energies of end members of solid solutions I–IV were evaluated according to the scheme described previously, based on equation 1, using the modeled chemical potentials of the relevant aqueous components and the measured stoichiometric coefficients.

Different limiting cases of carbonate concentration produce very similar ranges of total-scale Lippmann solubility products (Table 5). Hence, considering the end-member uncertainty ranges illustrated in Figure 10, the 'simple and idealized' stoichiometric formula number I was found to be sufficient to describe the hydrotalcite–pyroaurite solid solution.

However, results of this modeling revealed that the ideal solid solution model (see solidus and solutus curves in Figure 10a) with $\log\Sigma\Pi_T$ values of hydrotalcite and pyroaurite equal to −32.18 and −35.18, respectively, did not reproduce the intermediate compo-

Table 5. Stoichiometric formulae, standard molar Gibbs free energies, and total-scale Lippmann solubility products of hydrotalcite and pyroaurite end members evaluated from aqueous compositions after 140 days of dissolution experiments at 23±2ºC and pH = 11.40±0.03.

Solution no.	Solid solution composition	G^o_{298}(Htlc) (kJ/mol)	G^o_{298}(Pyraur) (kJ/mol)	$\log\Sigma\Pi_T$ Htlc	$\log\Sigma\Pi_T$ Pyraur
I	$Mg_3(Al,Fe)(OH)_8(CO)_{0.5}$	−3746.37	−3304.01	−32.18	−35.18
II	$Mg_3(Al,Fe)_{0.954}(OH)_{7.826}(CO_3)_{0.518}$	−3691.37	−3268.07	−30.77	−33.41
III	$Mg_3(Al,Fe)_{0.954}(OH)_{8.266}(CO_3)_{0.298}$	−3645.17	−3221.57	−30.92	−33.50
IV	$Mg_3(Al,Fe)_{0.954}(OH)_{8.046}(CO_3)_{0.408}$	−3668.17	−3244.87	−30.83	−33.46

https://doi.org/10.1346/CCMN.2011.0590301 Published online by Cambridge University Press

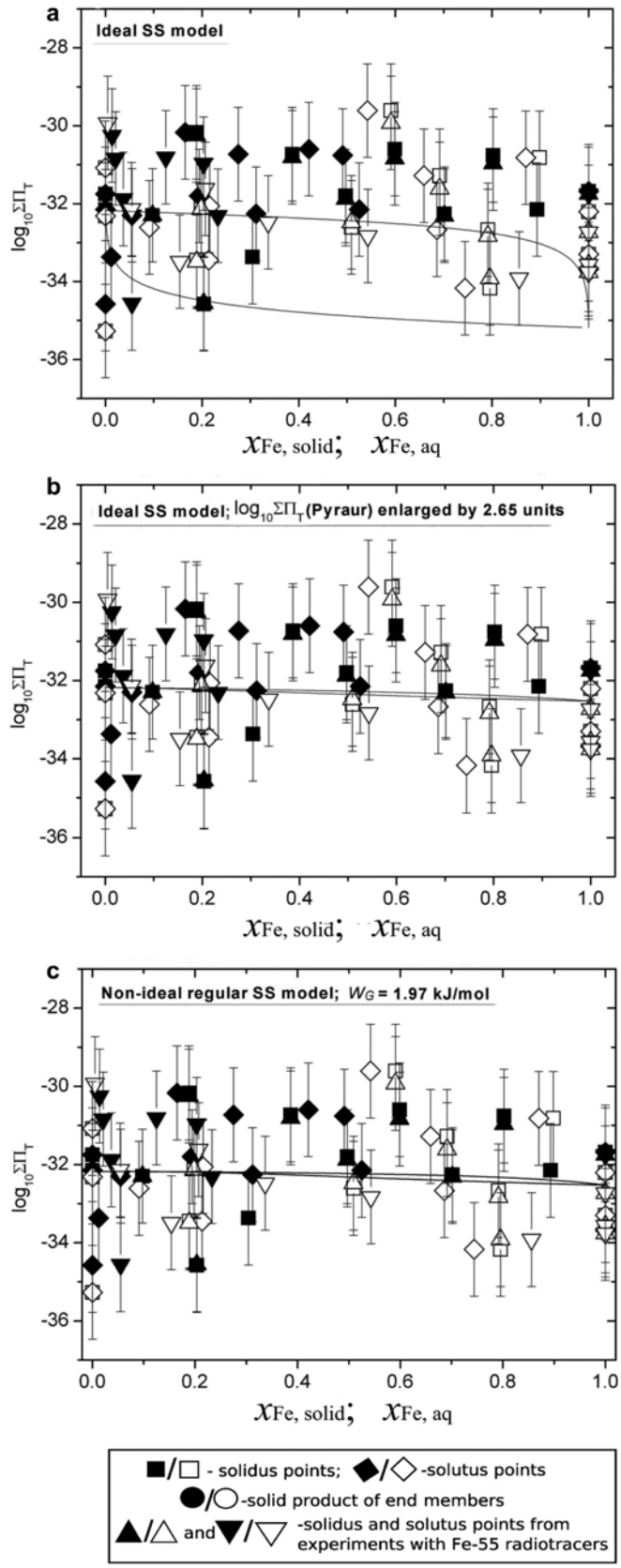

https://doi.org/10.1346/CCMN.2011.0590301 Published online by Cambridge University Press

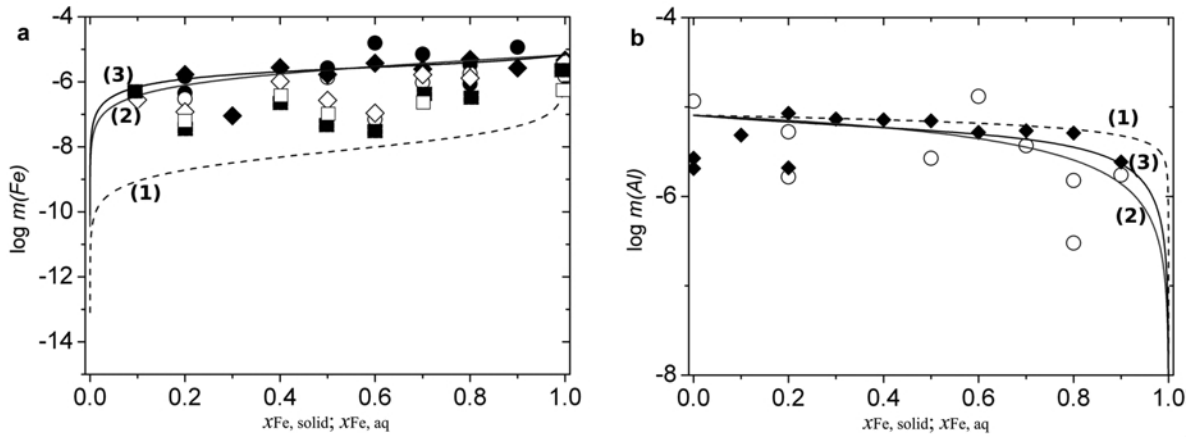

Figure 11. Total dissolved molalities of (a) Fe and (b) Al (using a logarithmic scale) as a function of the Fe/(Fe+Al) mole fraction in the hydrotalcite–pyroaurite solids. Filled symbols denote results of co-precipitation experiments. Empty symbols are results from solubility measurements. Squares represent the data obtained from experiments with radioactive ^{55}Fe tracers. Diamonds are concentrations determined by ICP-OES. Curve 1 corresponds to the ideal solid solution model, where G^{o}_{298}(Htlc) = −3746.37 kJ/mol and G^{o}_{298}(Pyraur)= −3304.01 kJ/mol. Curves 2 and 3 represent results obtained for the ideal solid solution and for a regular solid solution (W_G = 0.98 kJ/mol), respectively, where G^{o}_{298}(Htlc) = −3746.37 kJ/mol and G^{o}_{298}(Pyraur) = −3289.01 kJ/mol.

sitions very well. This mismatch was also illustrated in the isotherms in Figure 11a, where experimental Fe concentrations were compared to the model Curve 1.

The model fit can be improved, in principle, by adjusting the molar Gibbs free energies of hydrotalcite, pyroaurite, or both. In practice, however, varying the G^{o}_{298} value of hydrotalcite led to no improvements in the modeled Fe concentrations. The G^{o}_{298} value of pyroaurite was, therefore, adjusted to −3289.01 kJ/mol (corresponding to a solubility product of pyroaurite of −32.53) and the improved ideal-solution Curve 2 in Figure 11 was obtained.

Curve 2 does not represent the observed differences between the solidus and solutus data points very well. Thus, further attempts were made to improve the representation of measured concentrations by introducing some non-ideality in the form of a regular mixing model:

$$G^{EX} = W_G\, x_{Htlc}\, x_{Pyraur}$$

The solid-solution interaction parameter, W_G, was adjusted to best fit the differences between solidus and solutus points (*i.e.* $x_{Fe,\ solid} - x_{Fe,aq}$) for each individual experiment. This was performed by finding the interaction parameter, W_G, that minimizes the sum of squared residuals, S_1:

$$S_1 = \sum_{i=1}^{n} [(x\mathrm{Fe, solid} - x_{Fe,aq})_{experiment} - (x_{Fe,solid} - x_{Fe,aq})_{model}]^2 \ \rightarrow \ \min = 0.64$$

This exercise produced a slight improvement with a modest regular interaction parameter, W_G = 1.97 kJ/mol^{-1} (see also Curve B in Figure 12).

Another least-squares fit procedure was applied to improve the representation of Fe partitioning between the solid and liquid phases. In this case, the regular interaction parameter W_G was adjusted to best fit the measured aqueous mole fractions of Fe as a function of the mole fraction of Fe in solids, *i.e.* $x_{Fe,aq} = f(x_{Fe,solid})$ (Figure 12). The fitting procedure entailed finding a W_G value that minimized the sum of squared residuals, S_2:

$$S_2 = \sum_{i=1}^{n} [x_{Fe,aq}(\mathrm{experiment}) - x_{Fe,aq}(\mathrm{model})]^2 = 0.93$$

This led to the optimized interaction parameter W_G = 0.98 kJ/mol (Curve C in Figure 12).

Neither value of the interaction parameter produced a miscibility gap but both were still close to the ideal solid-solution behavior. Nevertheless, from examination of the curves B and C in Figure 12, the introduction of additional non-ideality into the model is clearly unjustified by the uncertainty of the data. Curves A, B, and C provide, in principle, the same results. In such a situation, it is reasonable to select the simplest, *i.e.* the simple ideal mixing model (Curve A).

Standard molar Gibbs free energies, absolute molar entropies, molar enthalpies, and absolute molar heat capacities of the end members at 298 K and 1 bar were

Figure 10 (*facing page*). Lippmann solubility diagram (using total concentration scale) of the hydrotalcite–pyroaurite aqueous solid solution system. (a) Ideal solid solution model with log$\Sigma\Pi_T$(Htlc) = 32.18 and log$\Sigma\Pi_T$(Pyraur) = −35.18; (b) ideal solid solution with log$\Sigma\Pi_T$(Htlc) = −32.18 and log$\Sigma\Pi_T$(Pyraur) = −32.53 (c) Non-ideal regular solid solution with log$\Sigma\Pi_T$(Htlc) = −32.18 and log$\Sigma\Pi_T$(Pyraur) = −32.53 and W_G = 1.97 kJ/mol.

https://doi.org/10.1346/CCMN.2011.0590301 Published online by Cambridge University Press

Table 6. Thermodynamic properties of hydrotalcite and pyroaurite end members.

Phase	G^{o}_{298} (kJ/mol)	S^{o}_{298} (J/(mol·K))	H^{o}_{298} (kJ/mol)	Cp^{o}_{298} (J/(mol·K))	V^{o}_{298} (cm^3/mol)	$\log K_f$	a	b	c	$\log\Sigma\Pi_T$
Hydrotalcite $Mg_3Al(OH)_8(CO_3)_{0.5}\cdot 2.5H_2O$	−4339.85	411.46	−4875.89	512.60	115.0	66.77±1.20	−556.59	30287.60	91.58	−32.18±1.20
Pyroaurite $Mg_3Fe(OH)_8(CO_3)_{0.5}\cdot 2.5H_2O$	−3882.60	422.51	−4415.09	521.27	119.0	68.04±1.20	−543.36	30562.50	89.32	−32.53±1.20

a, b, c: Coefficients of the equilibrium formation constant ($\log K_f$) expressed as $\log K_f = a + b/T + c\cdot\ln T$, derived from $\Delta_r G^o$, $\Delta_f H^o$, $\Delta_r S^o$, $\Delta_r Cp^o$ values of reactions 11 and 12 (see text for explanation). Sources of other data are given in Table 7.

Figure 12. Iron partitioning between the aqueous phase and the solid solution expressed in a Roozeboom diagram. Filled symbols show the results of co-precipitation experiments. Open symbols represent solubility-measurement data. Diamonds denote results based on ICP-OES measurements. Squares are results from experiments using ^{55}Fe radiotracers. Curve 1 represents partitioning of Fe in an ideal solid solution with G^{o}_{298}(Htlc) = −3746.37 kJ/mol and G^{o}_{298}(Pyraur) = −3304.01 kJ/mol. Curve A shows results obtained from the ideal solid solution model where G^{o}_{298}(Htlc) = −3746.37 kJ/mol and G^{o}_{298}(Pyraur) = −3289.01 kJ/mol. Curves B and C demonstrate partitioning of Fe in non-ideal regular solid solutions (G^{o}_{298}(Htlc)= −3746.37 kJ/mol and G^{o}_{298}(Pyraur) = −3289.01 kJ/mol with regular interaction parameters (W_G) equal to 1.97 and 0.98 kJ/mol, respectively).

estimated (Table 6). These estimates were based on thermodynamic data in the *NAGRA/PSI Chemical Thermodynamic Database* (Hummel, 2002; Majzlan *et al,.* 2003a, 2003b), as given in Table 7, including the data presented by Allada *et al.* (2005) for the thermochemical effect of hydrotalcite formation from carbonates and hydroxides.

To estimate the absolute molar entropies of the hydrotalcite and pyroaurite end members, the reactions by which hydrotalcite and pyroaurite decompose to carbonates and hydroxides were formulated:

$$Mg_3Al(CO_3)_{0.5}(OH)_8\cdot 2.5H_2O = 0.5Mg(CO_3)_{(s)} + 2.5Mg(OH)_{2(s)} + AlOOH_{(s)} + 3.5H_2O_{(l)} \quad (8)$$

$$Mg_3Fe(CO_3)_{0.5}(OH)_8\cdot 2.5H_2O = 0.5Mg(CO_3)_{(s)} + 2.5Mg(OH)_{2(s)} + FeOOH_{(s)} + 3.5H_2O_{(l)} \quad (9)$$

In order to adjust the values of the absolute molar entropy and molar heat capacity of the hydrotalcite end member, the entropy (265.46±0.52 J/mol·K) and heat capacity (340.28±0.50 J/mol·K)) of a specific hydrotalcite, $Mg_{2.277}Al_{0.87}(OH)_{6.154}(CO_3)_{0.4}\cdot 1.2H_2O$, investigated by Allada *et al.* (2005) using adiabatic calorimetry, were considered. Thus, formation of this solid solution from pure hydrotalcite can be represented by the following reaction:

$$0.8Mg_3Al(OH)_8(CO_3)_{0.5}\cdot 2.5H_2O = Mg_{2.277}Al_{0.8}(OH)_{6.154}(CO_3)_{0.4}\cdot 1.2H_2O_{(s)} + 0.123Mg(OH)_{2(s)} + 0.8H_2O_{(l)} \quad (10)$$

https://doi.org/10.1346/CCMN.2011.0590301 Published online by Cambridge University Press

Table 7. Standard molar Gibbs energies, absolute entropies, enthalpies, and absolute heat capacities of substances used in thermodynamic calculations.

Phase/formula	G^o_{298} (kJ/mol)	S^o_{298} (J/(mol·K))	H^o_{298} (kJ/mol)	Cp^o_{298} (J/(mol·K))	References
Boehmite/$AlOOH_{(s)}$	−908.97	48.45	−983.57	65.64	(1)
Brucite/$Mg(OH)_{2(s)}$	−832.23	63.14	−923.27	77.28	(1)
Goethite/$FeOOH_{(s)}$	−493.363	59.50	−564.40	74.31	(2)
Magnesite/$Mg(CO_3)_{(s)}$	−1029.28	65.69	−1112.89	75.85	(1)
Water/$H_2O_{(l)}$	−237.18	69.92	−285.88	75.36	(1)
$Mg_{2.277}Al_{0.87}(OH)_{6.154}(CO_3)_{0.4}\cdot 1.2H_2O$	−3205.72	265.46	−3584.44	340.28	(3)
$Al^{3+}_{(aq)}$	−483.71	−325.10	−530.63	−128.70	(1)
$Mg^{2+}_{(aq)}$	−453.99	−138.07	−465.93	−21.66	(1)
$Fe^{3+}_{(aq)}$	−17.19	−277.40	−49.58	−76.71	(1)

References: (1) Hummel *et al.* (2002); (2) Majzlan *et al.* (2003a, 2003b); (3) Allada *et al.* (2005).

As the reactant and product solids have similar structures, the approximation can be made (following Helgeson *et al.*, 1978) that $\Delta_r S^o$ and $\Delta_r Cp^o$ are zero. This approach yields the following values:

S^o_{298} (hydrotalcite) = 411.46±0.65 J/(mol·K),
Cp^o_{298} (hydrotalcite) = 512.60±0.62 J/(mol·K).

The apparent uncertainties given above for S^o_{298} (hydrotalcite) and Cp^o_{298} (hydrotalcite) are due solely to the errors in the data of Allada *et al.* (2005). The real uncertainties will be larger if the error incurred by assuming $\Delta_r S^o$ and $\Delta_r Cp^o = 0$ is taken into account.

Using the evaluated values of S^o_{298} (hydrotalcite) = 411.46±0.65 and Cp^o_{298} (hydrotalcite) = 512.60±0.62 J/(mol·K), the properties of reaction 8 were estimated to be $\Delta_r S^o$ = 72.41 ±0.65 and $\Delta_r Cp^o$ = 47.92 ±0.63 J/(mol·K). These values are not large, and they allow a three-term temperature extrapolation of $\Delta_r G^o$ up to 70ºC with an error of <0.3 pK units. Thus, the dependence of the reaction constant on temperature may be similarly expressed in the form of a three-term temperature approximation: $\log K(T) = a + b/T + c\cdot \ln T$, in which $a = -12.98$, $b = -670.14$, and $c = 2.50$.

The entropy and heat capacity of pyroaurite, $Mg_3Fe(OH)_8(CO_3)_{0.5}\cdot 2.5H_2O$, could not be estimated using the Helgeson method because of the lack of appropriate calorimetric data. For this reason, the entropy and heat capacity of pyroaurite were re-evaluated assuming that the entropy and heat capacity changes for reaction 9 are the same as for reaction 8.

S^o_{298} (pyroaurite) = 422.51±0.50 J/(mol·K)
Cp^o_{298} (pyroaurite) = 521.27±0.50 J/(mol·K)

The corresponding $\log K(T)$ approximation for reaction 9 was: $\log K(T) = a + b/T + c\cdot \ln T$, where $a = -12.98$, $b = 1504.74$, and $c = 2.50313$, leading to the dataset for 3:1 hydrotalcite and pyroaurite end members given in Table 6.

Using these thermodynamic data for hydrotalcite and pyroaurite in reactions including simple aqueous ions, the common expressions for the formation constants of the solids at 25ºC and 1 bar were obtained:

$$3Mg^{2+}_{(aq)} + Al^{3+}_{(aq)} + 8OH^-_{(aq)} + 0.5CO^{2-}_{3\,(aq)} + 2.5H_2O_{(l)} = Mg_3Al(OH)_8(CO_3)_{0.5}\cdot 2.5H_2O \quad (11)$$

with $\log_{10}K_{f,Htlc}$ = 66.77±1.20 and a three-term temperature approximation:

$$\log_{10}K_{f,Htlc}(T) = a + b/T + c\cdot \ln T$$

where $a = -556.59$, $b = 30287.60$, and $c = 91.58$;

$$3Mg^{2+}_{(aq)} + Fe^{3+}_{(aq)} + 8OH^-_{(aq)} + 0.5CO^{2-}_{3\,(aq)} + 2.5H_2O_{(l)} = Mg_3Fe(OH)_8(CO_3)_{0.5}\cdot 2.5H_2O \quad (12)$$

with $\log_{10}K_{f,Pyraur}$ = 68.04±1.20 and a three-term temperature approximation:

$$\log_{10}K_{f,Htlc}(T) = a + b/T + c\cdot \ln T,$$

where $a = -543.36$, $b = 30562.50$, and $c = 89.32$.

Expressions of this type are normally used in speciation codes such as *PHREEQC* (Parkhurst and Appelo, 1999).

The molar volumes of end members have been calculated by inserting the measured powder XRD data into the volumetric equation for the hexagonal crystal system ($V_{unit\ cell} = a_o^2 c_o \sin(60^o)$). The values obtained were converted to molar volumes *via* $V_m = N_A \times V_{unit\ cell}$, where N_A is the Avogadro constant (6.022×10^{23} mol^{-1}). This results in molar volumes of hydrotalcite and pyroaurite end members of 11.50 and 11.90 J/bar (115 and 119 cm^3/mol), respectively.

According to Miyata (1980) and Vagvolgyi *et al.* (2008), and considering the results of Rozov *et al*. (2010), the thermal decomposition and structural changes of hydrotalcite-like phases began with the loss of interlayer water at approximately 60–70ºC. The estimated standard molar entropies and heat capacities can, therefore, be used reliably up to these temperatures. An increase in temperature above 70ºC will lead to loss of interlayer water, decomposition of structural hydroxyl groups, and, finally, to loss of interlayer carbonate anions. Such

https://doi.org/10.1346/CCMN.2011.0590301 Published online by Cambridge University Press

behavior was observed by Vidal and Dubacq (2009) in layered smectite solid-solutions, which are broadly similar to the solids in the present study. Progressive dehydration should lead to progressive increase of the non-ideality of mixing, leading to miscibility gaps between 'pyrophyllite' and 'mica-like' phases. Conversely, hydration should facilitate mixing in layered clay structures, thereby making them closer to ideal solutions. A similar evolution can be expected for the hydrotalcite–pyroaurite solid-solution series. Hence, the ideal solid-solution model, as well as the regular solid-solution behavior with small interaction parameter $0.97 < W_G < 1.97$ kJ/mol, is expected to be valid for temperatures between 0 and 70ºC and pressures <100 bar.

SUMMARY AND CONCLUSIONS

The aim of the present work was to estimate the stabilities of the LDH end members hydrotalcite and pyroaurite, and to estimate the aqueous solubility of hydrotalcite–pyroaurite solid solutions by combining the results of co-precipitation and dissolution experiments.

Synthetic hydrotalcite–pyroaurite solids with initial $Mg^{II}/(Al^{III}+Fe^{III})$ mole ratios of ~3:1 were studied in co-precipitation (Rozov *et al.*, 2010) and dissolution experiments in alkaline aqueous environments (pH = 11.40±0.03) at ambient conditions (23±2ºC, 1 bar).

The results of the dissolution experiments reported here show that the post-experimental $Mg^{II}/(Al^{III}+Fe^{III})$ ratios measured in the solid phases were 3.09±0.11 (Table 2), whereas $Mg^{II}/(Al^{III}+Fe^{III})$ ratios in aqueous solutions were ~3.60±1.47 (Table 1). The ranges of uncertainties in both ratios encompass the value 3.00 and so do not contradict the congruent dissolution behavior of hydrotalcite–pyroaurite solids, and are, therefore, consistent with the absence of significant amounts of secondary phases (*i.e.* gibbsite, magnesite, brucite, and Fe hydroxides). Furthermore, no decrease in the crystallite size after 140 days of dissolution was observed, indicating that the system approached equilibrium or at least stoichiometric saturation.

All the measured powder XRD patterns demonstrated the presence of hydrotalcite-like phases only. This means that possible amounts of conceivable impurities (like gibbsite, brucite, magnesite, or Fe hydroxide) did not exceed the detection limit of the X-ray diffraction technique (~5–6 wt.%). Unit-cell distances $a_o = b_o$ of hydrotalcite and pyroaurite end members did not change significantly during the 140 days of the dissolution experiment. The M^{II}/M^{III} ratio in the brucite-like layer remained constant. Over the same time period, the very small observed changes in the c_o parameter may indicate some insignificant rearrangements in the interlayer (perhaps substitutions of carbonate by hydroxide).

Standard molar Gibbs free energies, G^o_{298}, of hydrotalcite and pyroaurite end members (and molar Gibbs free energies, G_{298}, of intermediate phases) were evaluated assuming that solid and aqueous phases were in thermodynamic equilibrium. However, this evaluation was hampered by the uncertainties in the analysis of the solid phases. Excluding the interlayer water, each solid consisted of five components, four of which are known only within the ranges of analytical uncertainty (the fifth is given by electroneutrality). This means that a range of compositions is compatible with the actual analytical data. This 'valid' compositional range leads to uncertainties of ~±103 kJ/mol in the calculated molar Gibbs free energies. If analytical uncertainties are ignored and the compositions of the solids are taken as analyzed, much smaller uncertainties of ~2–3 kJ/mol are calculated, arising mainly from analytical uncertainties of the aqueous solutes.

The results of co-precipitation and dissolution experiments using ^{55}Fe radiotracers yielded no significant improvement, the reason being that only concentrations of dissolved Fe were analyzed in the traced solutions, whereas concentrations of other ions (*i.e.* Mg^{2+}, Al^{3+}, Na^+, CO_3^{2-}, OH^-) and stoichiometric compositions were assumed to be the same as in experiments without ^{55}Fe. The results of the radiotracer experiments, in general, confirmed the results from ordinary ICP-OES measurements.

The total-scale Lippmann solubility products, $\Sigma\Pi_T$, were evaluated directly from experimental solubility data for ~40 samples with various Fe/(Fe+Al) ratios and slightly different $Mg^{II}/(Al^{III}+Fe^{III})$ ratios. From subsequent fitting exercises, with adjustment of the G^o_{298} values of hydrotalcite and pyroaurite end members using Lippmann diagrams, isotherms, and Roozeboom diagrams, a simple ideal solid-solution model with similar end-member $\Sigma\Pi_T$ values was sufficient to reproduce the measured aqueous concentrations over the full range of intermediate compositions. Applying non-ideal (regular) solid-solution models did not significantly improve the results because of the substantial scattering and large uncertainties in the experimental data for the partitioning of Fe. Both the simple ideal mixing model and a regular model with interaction parameter $W_G < 2$ kJ/mol (optimally 0.98 kJ/mol) described the solubility data equally well.

The present study provides the first estimates of G^o_{298} (−3882.60±2.00 kJ/mol) and of the equilibrium formation constant from aqueous ions ($\log K_f$ = 68.04±1.2) of pure 3:1 carbonate pyroaurite. The values are consistent both with $\log K_f$ = 66.77±1.2 and G^o_{298} = −4339.85 kJ/mol of pure 3:1 carbonate hydrotalcite, and with the whole series of solid solutions having intermediate mole fractions of Fe.

Applying the method of Helgeson *et al.* (1978) and using thermodynamic data from adiabatic calorimetry (Allada *et al.*, 2005) for a hydrotalcite with formula $Mg_{2.277}Al_{0.8}(OH)_{6.154}(CO_3)_{0.4}\cdot 1.2H_2O$, new values of standard entropy (411.46 J/(mol·K)) and heat capacity (512.60 J/(mol·K) were estimated for the hydrotalcite

https://doi.org/10.1346/CCMN.2011.0590301 Published online by Cambridge University Press

end member $Mg_3Al(OH)_8(CO_3)_{0.5}\cdot 2.5H_2O$. The corresponding standard entropy and heat capacity for pyroaurite (S^o_{298} = 422.51 and Cp^o_{298} = 521.27 J/(mol·K), respectively) were estimated assuming that the decomposition of pyroaurite to hydroxide minerals and water (equation 9) behaves similarly to the decomposition of hydrotalcite (equation 8). The new estimated values of entropy and heat capacity of pure end members are likely to be valid within the temperature/pressure ranges of 0–70ºC and 1–100 bar.

In the present modeling of the solubility of hydrotalcite–pyroaurite phases, the largest remaining uncertainty factor is the missing consideration of the $Mg^{II}/(Al^{III}+Fe^{III})$ cationic ratio, which was taken here to be 3:1. In reality, however, measured solid compositions result in somewhat variable ratios: 2.94±0.2 in co-precipitation experiments and 3.07±0.3 in dissolution experiments. Various M^{II}/M^{III} ratios have been reported in the literature, and hydrotalcite-like LDH phases can be synthesized at any cationic ratio between about 2 and 4 (Cavani *et al.*, 1991; Khan and O'Hare, 2002; De Roy, 1992). Because of this, the dependence of stability/solubility of hydrotalcite–pyroaurite solids on the $Mg^{II}/(Al^{III}+Fe^{III})$ ratio was further investigated here and a more sophisticated solid-solution model was developed with end members having different cationic ratios. These results and a critical comparison with literature data on hydrotalcite will be presented elsewhere.

ACKNOWLEDGMENTS

The authors thank Dr. U. Eggenberger, C. Wanner, and M. Fisch (University of Bern) for their help with the powder XRD analyses; G. Lambrecht for support with Raman spectroscopy; A. Frei (Paul Scherrer Institute) and B. Dilnesa (EMPA) for support with TGA; Dr. J. Tits and D. Kunz (Paul Scherrer Institute) for their support with ^{55}Fe radiotracers; S. Koechli (Paul Scherrer Institute) for support with ICP-OES measurements; Dr. Z. Berner and C. Moessner (University of Karlsruhe) for ICP-MS control analyses of Fe; and the Swiss National Cooperative for the Disposal of Radioactive Waste (NAGRA) for financial support.

REFERENCES

Allada, R.K., Navrotsky, A., and Boerio-Goates, J. (2005) Thermochemistry of hydrotalcite-like phases in the MgO-Al_2O_3-CoO_2-H_2O system: A determination of enthalpy, entropy and free energy. *American Mineralogist*, **90**, 329–335.

Allmann, R. (1968) Crystal structure of pyroaurite. *Acta Crystallographica. Section B. Structural Crystallography and Crystal Chemistry*, **B 24**, 972.

Bish, D.L. and Howard, S.A. (1988) Quantitative phase-analysis using the Rietveld method. *Journal of Applied Crystallography*, **21**, 86–91.

Brindley, G.W. and Kikkawa, S. (1979) A crystal-chemical study of Mg, Al and Ni, Al hydroxy-perchlorates and hydroxy-carbonates. *American Mineralogists*, **64**, 836–843.

Brindley, G.W. and Kikkawa, S. (1980) Thermal-behavior of hydrotalcite and of anion-exchanged forms of hydrotalcite. *Clays and Clay Minerals*, **28**, 87–91.

Carrado, K.A., Kostapapas, A., and Suib, S.L. (1988) Layered double hydroxides (LDHs). *Solid State Ionics*, **26**, 77–86.

Cavani, F., Trifiro, F., and Vaccari, A. (1991) Hydrotalcite-type anionic clays: Preparation, properties and applications. *Catalysis Today*, **11**, 173–301.

Chibwe, K. and Jones, W. (1989) Intercalation of organic and inorganic anions into layered double hydroxides. *Journal of the Chemical Society – Chemical Communications*, 926–927.

Chisem, I.C. and Jones, W. (1994) Ion-exchange properties of lithium aluminum layered double hydroxides. *Journal of Materials Chemistry*, **4**, 1737–1744.

Danton, A.R. (1991) Vegard's law. *Physical Review*, **43**, 3161–3164.

De Roy, A., Forano, C., El Malki, M., and Besse, J.-P. (1992) *Anionic clays: Trends in Pillaring Chemistry*. Van Nostrand Reinhold, New York.

Drits, V.A. and Bookin, A.S. (2001) Crystal structure and X-ray identification of layered double hydroxides. Pp. 41–100 in: *Layered Double Hydroxides. Present and Future* (V. Rives, editor). Nova Science Publishers, New York.

Drits, V.A., Sokolova, T.N., Sokolova, G.V., and Cherkashin, V.I. (1987) New members of the hydrotalcite-manasseite group. *Clays and Clay Minerals*, **35**, 401–417.

Frost, R.L. and Reddy, B.J. (2006) Thermo-Raman spectroscopic study of the natural layered double hydroxide manasseite. *Spectrochimica Acta. Part A. Molecular and Biomolecular Spectroscopy*, **65**, 553–559.

Gutmann, N. and Müller, B. (1996) Insertion of the dinuclear dihydroxo-bridged Cr(IV) aquo complex into the layered double hydroxides of hydrotalcite-type. *Journal of Solid State Chemistry*, **122**, 214–220.

Helgeson, H.C., Delany, J.M., Nesbitt, H.W., and Bird, D.K. (1978) Summary and critique of the thermodynamic properties of rock-forming minerals. *American Journal of Science*, **278A**, 1–229.

Hummel, W. (2002) *Nagra/PSI Chemical Thermodynamic Database 01/01*. Universal-Publishers, Parkland, Florida, USA, 589 pp.

Johnson, C.A. and Glasser, F.P. (2003) Hydrotalcite-like minerals ($M_2Al(OH)_6(CO_3)_{0.5}\cdot nH_2O$, where M = Mg, Zn, Co, Ni) in the environment: Synthesis, characterization and thermodynamic stability. *Clays and Clay Minerals*, **51**, 1–8.

Khan, A.I. and O'Hare, D. (2002) Intercalation chemistry of layered double hydroxides: Recent developments and applications. *Journal of Materials Chemistry*, **12**, 3191–3198.

Kovanda, F., Koulousek, D., Cilova, Z., and Hulinski, V. (2005) Crystallization of synthetic hydrotalcite under hydrothermal conditions. *Applied Clay Science*, **28**, 101–109.

Lippmann, F. (1980) Phase diagrams depicting aqueous solubility of binary mineral systems. *Neues Jahrbuch für Mineralogie Abhandlungen*, **139**, 1–25.

Majzlan, J., Grevel, K.D., and Navrotsky, A. (2003a) Thermodynamics of Fe oxides: Part II. Enthalpies of formation and relative stability of goethite (α-FeOOH), lepidocrocite (γ-FeOOH), and maghemite (γ-Fe_2O_3). *American Mineralogist*, **88**, 855–859.

Majzlan, J., Lang, B.E., Stevens, R., Navrotsky, A., Woodfield, B.F., and Boerio-Goates, J. (2003b) Thermodynamics of Fe oxides: Part I. Entropy at standard temperature and pressure and heat capacity of goethite (α-FeOOH), lepidocrocite (γ-FeOOH), and maghemite (γ-Fe_2O_3). *American Mineralogist*, **88**, 846–854.

Miyata, S. (1975) The syntheses of hydrotalcite-like compounds and their structures and physico-chemical properties. *Clays and Clay Minerals*, **23**, 369–375.

Miyata, S. (1980) Physicochemical properties of synthetic

hydrotalcites in relation to composition. *Clays and Clay Minerals*, **28**, 50–56.

Miyata, S. (1983) Anion-exchange properties of hydrotalcite-like compounds. *Clays and Clay Minerals*, **31**, 305–311.

Parkhurst, D.L. and Appelo, C.A.J. (1999) *User's guide to PHREEQC* (version 2). Pp. 99–4259. US Geological Survey Water Resources Investigations Report.

Prikhod'ko, R.V., Sychev, M.V., Astrelin, I.M., Erdmann, K., Mangel, A., and van Santen, R.A. (2001) Synthesis and structural transformations of hydrotalcite-like materials Mg-Al and Zn-Al. *Russian Journal of Applied Chemistry*, **74**, 1621–1626.

Rozov, K., Berner, U., Taviot-Gueho, C., Leroux, F., Renaudin, G., Kulik, D., and Diamond, L.W. (2010) Synthesis and characterization of the LDH hydrotalcite-pyroaurite solid solution series. *Cement and Concrete Research*, **40**, 1248–1254.

Trave, A., Selloni, A., Goursot, A., Tichit, D., and Weber, J. (2002) First principles study of the structure and chemistry of Mg-based hydrotalcite-like anionic clays. *Journal of Physical Chemistry*, **106**, 12291–12296.

Vagvolgyi, V., Palmer, S.J., Kristof, J., Frost, R.L., and Horvath, E. (2008) Mechanism for hydrotalcite decomposition: A controlled rate thermal analysis study. *Journal of Colloid and Interface Science*, **318**, 302–308.

Vidal, O. and Dubacq, B. (2009) Thermodynamic modelling of clay dehydration, stability and compositional evolution with temperature, pressure and H_2O activity. *Geochimica et Cosmochimica Acta*, **73**, 6544–6564.

(*Received 31 March 2011; revised 20 May 2011; Ms. 561; A.E. J.D. Fabris*)